Construction and test of the final CMS Barrel Drift Tube Muon Chamber prototype

M. Aguilar-Benítez[a], J. Alberdi[a], M. Arneodo[b], K. Banicz[c], M. Benettoni[d], A. Benvenuti[e], S. Bethke[c], M. Cerrada[a,*], R. Cirio[b], N. Colino[a], E. Conti[d], M. Dallavalle[e], M. Daniel[a], D. Dattola[b], F. Daudo[b], M. De Giorgi[d], U. Dosselli[d], A. Fanfani[e], C. Fanin[d], M.C. Fouz[a], F. Gasparini[d], U. Gasparini[d], P. Giacomelli[e], V. Giordano[e], F. Gonella[d], C. Grandi[e], P. Guaita[d], M. Guerzoni[e], S. Lacaprara[d], I. Lippi[d], S. Marcellini[e], J. Marín[a], R. Martinelli[d], S. Maselli[b], A. Meneguzzo[d], E. Migliore[b], J. Mocholí[a], V. Monaco[b], A. Montanari[e], C. Montanari[e], F. Odorici[e], J.C. Oller[a], S. Paoletti[d], M. Passaseo[d], M. Pegoraro[d], C. Peroni[b], J. Puerta[a], H. Reithler[c], A. Romero[b], L. Romero[a], P. Ronchese[d], A.M. Rossi[e], T. Rovelli[e], R. Sacchi[b], J.M. Salicio[a], A. Staiano[b], T. Steinbeck[c], E. Torassa[d], R. Travaglini[e], L. Ventura[d], S. Ventura[d], A. Vitelli[b], F. Voetee[c], M. Wegner[c], C. Willmott[a], P. Zotto[f], G. Zumerle[d]

[a] CIEMAT-División de Física de Partículas, Avenida Complutense 22, E-28040 Madrid, Spain
[b] Universitat di Torino e Sez. dell' INFN, Torino, Italy
[c] III. Physikalisches Institut der RWTH Aachen, Germany
[d] Universitat di Padova e Sez. dell' INFN, Padova, Italy
[e] Universitat di Bologna e Sez. dell' INFN, Bologna, Italy
[f] Politecnico di Milano e Sez. dell' INFN, Padova, Italy

Abstract

A prototype of the CMS Barrel Muon Detector incorporating all the features of the final chambers was built using the mass production assembly procedures and tools. The performance of this prototype was studied in a muon test beam at CERN and the results obtained are presented in this paper. © 2002 Elsevier Science B.V. All rights reserved.

PACS: 29-40. Gx

Keywords: CMS; Muon chambers; Drift tubes

*Corresponding author. Tel.: + 34-91-346-6073; fax: + 34-91-346-6068.
E-mail address: cerrada@ciemat.es (M. Cerrada).

1. Introduction

By the end of 1998 some changes to the design of the CMS Barrel Muon Drift Tube Chambers [1]

were introduced. The main one, described in more detail below, affected the configuration of the drift cell cathodes. A new prototype, called Q4 as an acronym of the fourth Quadruplet prototype, was assembled at CIEMAT (Madrid) in 1999 in order to validate the new design and, in addition, to test the performance of the first construction line equipped with the final production tools. A check of the achievable precision and overall chamber quality, as well as a check of assembly procedures and an evaluation of the needed time and manpower, was mandatory to confirm the schedule and chamber construction planning.

Q4 is also the first prototype fully equipped with a preproduction sample of the final Front End electronics designed in Padova [2] and read out by a prototype of the final Readout Board [3] based on the 32-channel TDC designed at CERN [4]. In July 1999, the Q4 prototype was exposed to a muon test beam in the H2 experimental area at CERN.

In the following sections, the main features of the CMS Barrel Drift Tube Chambers are briefly described. A detailed discussion of the improvements introduced with the new design is made. The basic assembly and quality control procedures used in the construction of Q4, including mechanical and electrical tests, are reviewed. Finally, the results obtained from the analysis of the test beam data are presented.

2. The CMS Barrel Muon Drift Tube Chambers

The chambers are described in detail in the Technical Design Report [1]. Their performance was tested with several prototypes [5–7]. The CMS Barrel Muon Detector consists of four stations, called MB1–MB4, made of chambers with dimensions ranging from 2×2.5 m^2 for the innermost station, MB1, to 4×2.5 m^2 for the outermost one, MB4. The chambers are made of three independent units, or superlayers (SL), glued together and to a thick honeycomb plate as shown in Fig. 1. In each SL there are four layers of drift tubes (with a tube cross-section of 42×13 mm^2). All the wires inside a SL are parallel, and those of the even layers are staggered by half of the pitch with respect to those of the odd layers. Two SLs (ϕ type) measure the coordinate in the CMS bending plane and the third one (θ type) measures the coordinate along the beam direction. The θ type SL will not be available in MB4.
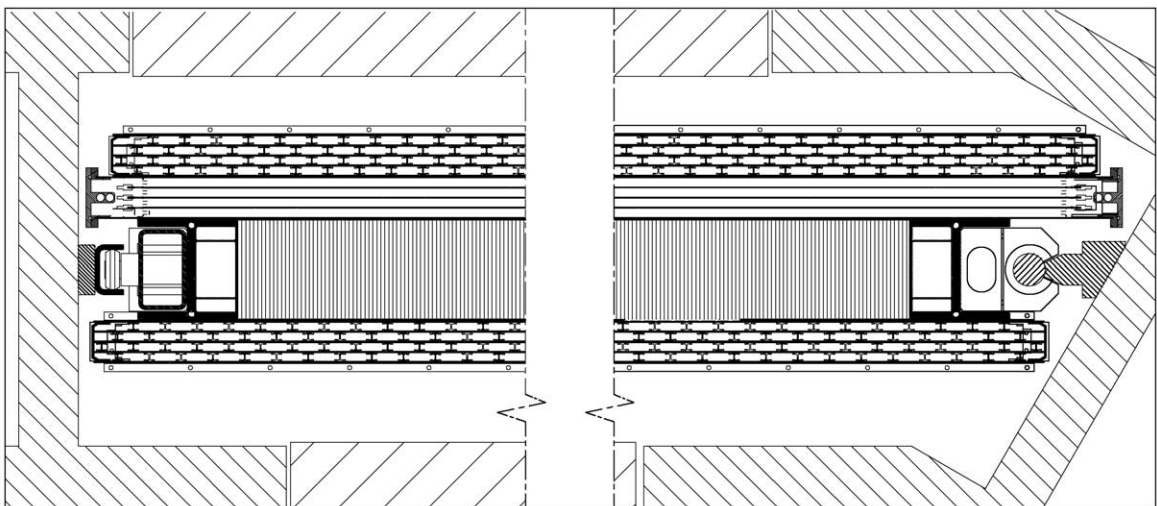

Fig. 1. Cut view of a drift tube chamber in its final position inside the CMS iron yoke. Two superlayers with wires along the beam direction and a third crossed one can be seen as well as the honeycomb panel providing rigidity to the chamber.

The mechanical precision required for the SL relative positions within a chamber is 0.5 mm. More strict tolerances are needed for the wires inside a SL. In order to meet the requirements on offline reconstruction momentum resolution and trigger, the wire pitch in a layer and the staggering from layer to layer must not deviate from nominal values by more than 100 μm. Assembly procedures have been developed to ensure that this mechanical precision is achieved and, in addition, it should be controlled during construction by measuring the position of each wire. These measured wire positions are recorded onto a data base.

3. The new drift cell design

A sketch of the cell showing drift lines can be seen in Fig. 2 for both the old design [1] and the new one used in Q4. Minor design changes are the following ones: the wire pitch was increased from 40 to 42 mm in order to optimize the electronics segmentation and the acceptance; the thickness of the grounded aluminium plates, at the top and bottom of the drift cells in Fig. 2, was decreased from 2 to 1.5 mm; the width of the electrode strip was changed from 14 to 16 mm in order to

optimize the electric field shaping; and the 50 μm diameter stainless steel anode wire is now gold plated.

The major design change is the new configuration of the cathode I-beams. In the old version, the aluminium beam itself was insulated from the aluminium plates by two plastic (Lexan) profiles and set to high voltage to act as a cathode. This solution provided good electrical results but some mechanical weakness was found during mechanical tests of chamber mockups [8]. In the new design, the I-beam has wider wings which increase the glue joint surface, and is glued directly to the aluminium plates. The number of structural glueings is therefore reduced by half and their strength improved. The mechanical behaviour of the new configuration was tested and found fully satisfactory.

As shown schematically in Fig. 3, cathodes are now placed on both sides of the I-beams following a technique similar to the one used for the strip electrodes on the aluminium plates. A cathode consists of a 50 μm thick, 11.50 mm wide aluminium tape insulated from the I-beam by a 19 mm wide, 100 μm thick mylar tape. This design allows for at least 3.5 mm separation of the electrode from the sides of the grounded I-beam. At the extremities the mylar tape is cut flush with respect to the I-beam ends while the aluminium tape is recessed by 5 mm. Both conductive and insulating ribbons are made self-adhesive with a pressure activated glue. Special tools were designed and built to glue them to both the plates and the I-
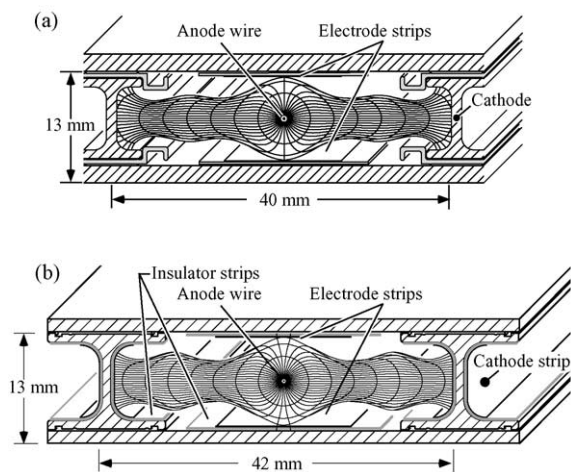

Fig. 2. Sketch of a cell showing drift lines and isochrones: (a) corresponds to the old design [1], and (b) corresponds to the new design used in Q4. The plates at the top and bottom of the cell are at ground potential.
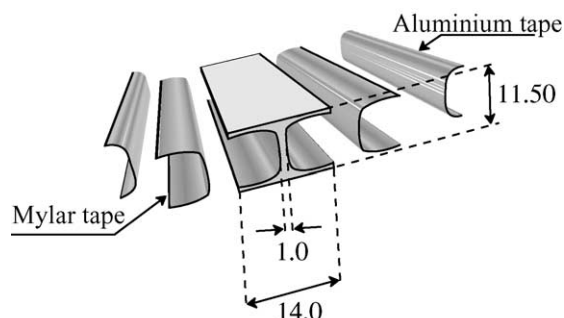

Fig. 3. Schematic exploded view of the cathode I-beam configuration in the new design. Dimensions are in mm.
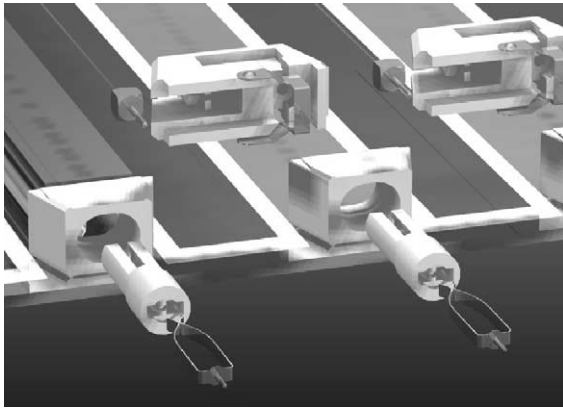
Fig. 4. Exploded view of the end part of the drift cells showing the different endplugs and spring contacts for high voltage connections.

Fig. 5. Calculated drift velocity (in μm/ns) as a function of the electric field (in kV/cm) for a gas mixture Ar/CO_2 (85/15%). Values obtained are very similar for the two different environment pressures, 730 and 770 Torr, shown in the figure.

Fig. 6. Equipotential lines in half of a drift cell with the new design configuration. The anode wire is at the right-hand side. The lines are labelled with the potential in volts.

beams. The only difference between the tapes used for the electrode strips and the ones just described is the width: the mylar tape used for the electrode strips is 23 mm wide and the aluminium tape is 16 mm wide. These strips are set to a positive voltage and contribute to improve the shaping of the electric field and the linearity of the space–time relation, most noticeably in the presence of magnetic fields.

Another consequence of the new I-beam design was the need to introduce, as a protection against discharges from the border at the ends of the cathode strips, a modification of the endplug plastic pieces which house the wire holders. The new pieces protrude inside the cell providing 12 mm of additional protection around the wire. I-beam and wire endplug pieces are shown in Fig. 4, as well as the springs connecting the electrodes to the high voltage.

The chambers are operated with an Ar–CO$_2$ (85/15%) mixture in order to avoid dealing with organic flammable gases and to have a small Lorenz angle in the presence of stray magnetic fields. This gas mixture and the drift cell optics described above allow to get a linear relationship between time and drift path. This is an essential requirement for the use of the chamber as a first level trigger device [9]. A calculation of the drift velocity using GARFIELD [10] is shown in Fig. 5. It can be seen that drift velocity saturation occurs between 1 and 2 kV/cm.
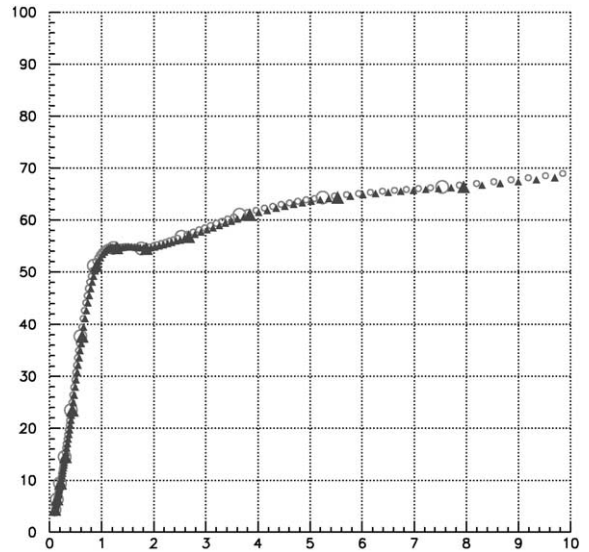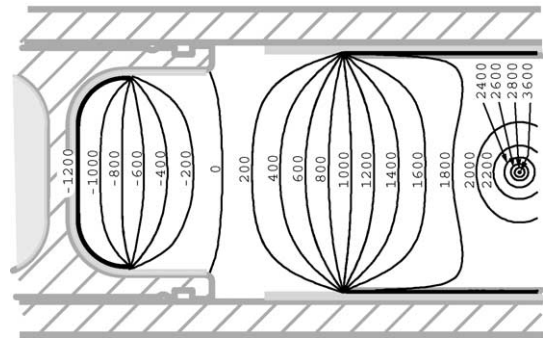
A gas gain around 10^5 was chosen to operate the drift cells. This gain allows to work within the efficiency plateau with a wide threshold range, which is convenient for the operation of large chambers in the environment expected at CMS.

The computation of equipotential lines (see Ref. [11]) displayed in Fig. 6 is useful to understand better the role of each electrode. The position of the zero voltage equipotential in the

region between the central strips and the cathodes is mainly determined by the size of the electrodes and not by their voltage values. The gas gain is mainly determined by the voltage drop from the wire (W) to the nearest electrode, the strips (S). The W–S voltage (V_{ampl}) must be kept between 1.75 and 1.85 kV in order to achieve a gain not far from the expected value of 10^5. Under the rough assumption of a uniform drift field of 1.5 kV/cm, the distances between the various electrodes imply that the strips should be set at a voltage larger or equal to 1.7 kV and the cathodes around −1 kV. As described below, during the chamber test at CERN, satisfactory performance was obtained with the voltages of cathodes, strips and wires respectively set to −1.2, + 1.8 and +3.6 kV.

4. Q4 construction and tests

Q4 is a narrow MB2 type superlayer with only 64, 2.5 m long wires (four layers of 16 wires each). The width was kept small to allow the insertion of Q4 inside the M1 magnet of the H2 beam line at CERN. It was built at CIEMAT in 1999 using the tools and assembly procedures described below which were developed for MB2 chamber production. Although the period of construction was about one month, the time dedicated to assembly amounted to 9 working days, according to the expected mass production schedule. The other basic parameter in the chamber construction planning, and manpower needs, was also checked by limiting the number of persons to three in the assembly work.

The I-beams for Q4 were prepared in Bologna, by means of a prototype of the mass production tool, and the plates in Madrid using a prototype ribbon dispenser designed and produced in Torino. The construction of Q4 was also a first test of the performance of these devices.

4.1. Superlayer assembly

A full layer of I-beams, equipped to act as drift tube cathodes, is glued in a single operation on top of a large aluminium plate. The aluminium plate is prepared in advance equipping it with the strip electrodes. At both ends of each I-beam, the plastic endplugs are also glued at the same time. Their shape allows an easy positioning of the other type of endplugs housing the wire holders. The positioning precision of the wire is guaranteed by the precise location of the I-beam endplugs (order of 50 μm) and by the mechanical precision of the moulded wire endplug pieces (order of 20 μm). Preliminary work is required before wires are inserted in all cells. Wire preparation includes stretching to achieve the right tension at the nominal length and crimping in their small Cu–Te holders. This operation is done using an automatic tool designed and built at Aachen. The wire position is measured by a CCD camera and the mechanical tension is checked by a special resonant circuit. When glueing the next aluminium plate to close the layer, a drop of conductive glue is placed on top of all I-beams to ensure a good grounding. This procedure is repeated four times to make a superlayer.

At a temperature of 20°, the two-component epoxy glue used needs 12 h for curing (nights are devoted to this). Therefore, assembly time is set by the number of glueing operations, leading to 9 days per superlayer.

The two outer plates, top and bottom, of the superlayer, are longer than the wires to create a volume for installing the High Voltage distribution boards at one end and Front End amplifiers at the other one. All this electronics is inside the gas volume to minimize the electronics noise. The lateral gas enclosures are glued once the fourth layer is ready and before closing the superlayer with the fifth aluminium plate. At this point, the superlayer is ready to be tested with gas and high voltage before being used to assemble the full chamber.

This procedure requires that each chamber assembly centre is equipped with production lines each one consisting of at least the following basic tools:

- Precision tables, larger than the corresponding chamber dimensions, and flat within 100 μm, instrumented with a glue dispenser capable of depositing glue cordons with the right amount of glue on the required locations. A system

based on a CCD camera should allow to measure wire positions, with better than 50 µm precision, and record them in a data base.

- I-beam and endplug holding tools to keep a full layer in the nominal position during the glueing operation.
- One machine to stretch and crimp the wires and one system to measure the wire tension during assembly.

In CMS, there will be four research institutes acting as superlayer and chamber assembly centres. RWTH–Aachen, CIEMAT, and Legnaro will have three assembly lines in order to build in parallel, the three superlayers which make up a chamber. In Torino an additional assembly line will be used to build MB4 chambers. Three other institutes participating in the CMS Barrel Muon Detector will take care of preparing aluminium plates, cathode I-beams and High Voltage boards.

4.2. Quality control

A preliminary quality control program prepared by the Collaboration was applied during the Q4 assembly process. It was based on the experience gained with the MB96 prototype construction [7] in Legnaro. The aim is to develop a protocol to be followed in each production centre to ensure the quality of the final chambers.

An important task in this process is the precise measurement of the wire positions. As shown in Fig. 7, the relative position of the wires in all layers of Q4 is well inside the allowed tolerances. The staggering between odd and even layers turned out to differ from the nominal value by about 500 µm. The origin of this problem was traced back to a wrong procedure used in positioning the I-beam tool with respect to the precision table reference system. It has been solved later on. All the other mechanical controls were satisfactory.

Once the superlayer was finished, a high voltage test was performed in air. Values of -2, $+2$ and $+4$ kV were applied to cathode, strips and wires respectively. The chamber was then closed and filled with gas to check gas tightness. O_2 contamination of the gas exiting from the chamber was
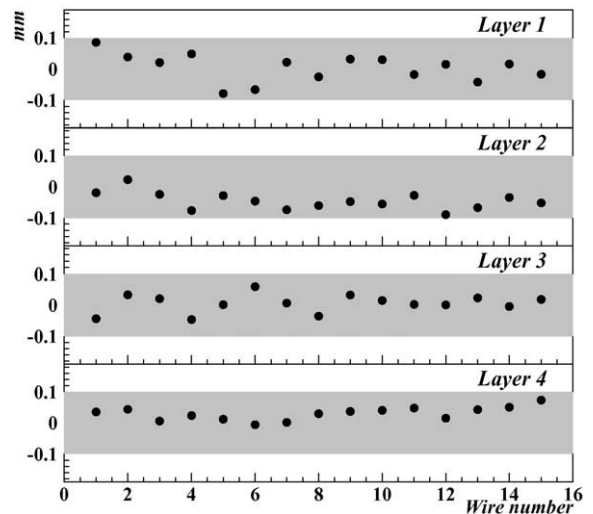

Fig. 7. Deviations from the nominal pitch of wires in each of the Q4 layers from measurements using a CCD camera as explained in the text. In all cases, the wires are inside the ± 100 µm window as required.

measured to be below 100 ppm after 24 h at a gas flow corresponding to 15 volume changes per day.

High voltage tests were repeated with the standard Ar–CO_2 (85/15%) mixture. In order to test the robustness of the new cathode design, negative voltages much higher than required were applied. MB96 operating values, -1.8, $+1.8$, $+3.6$ kV, could be reached with the exception of one cathode which failed. It was later discovered that the failure was due to the HV spring contact. Once it was replaced all cathodes passed the test.

Rates and TDC spectra, using a cosmic ray trigger, were obtained thus showing the correct operation of all the connected cells. The complete set of tests, before the shipment of Q4 to CERN, took one week.

5. Test beam results

5.1. Experimental set-up

Q4 was installed inside the M1 magnet of the CERN H2 zone in the SPS North Area in July 1999 and was exposed to a muon beam with

energies in the range 200–300 GeV. The chamber support allowed translations and rotations. The Q4 Front End electronics was based on engineering samples of a custom chip named MAD [2]. Front End Boards include four chips, each of the chips serving four channels. Wire signals are amplified and discriminated against an external threshold; then stretched and converted to LVDS compatible level in order to drive the long twisted pair cables to the acquisition chain. The readout system was based on the 32-channel general purpose TDC [4], with a bin size of 0.78 ns at 40 MHz. Four TDCs were implemented in a Readout Board (ROB). Data were transferred to a FIFO memory in a VME module with essentially no dead time. The VME memory was read out by the data acquisition system from a PC via a PCI–VME interface at the end-of-spill or after a programmable number of events. The ROB is also programmed and controlled through VME.

Information from a silicon beam telescope (SiBT) [12], located 2 m upstream of Q4, could be used to compare with the Q4 measurements. The SiBT has its own readout system. In order to synchronize the Q4 and SiBT data flows, the Q4 trigger was defined by the beam trigger coming from a set of scintillator counters plus a signal from SiBT DAQ. The spill number and the event number inside the spill were recorded by the two DAQs independently and were used to match the data from both systems in the offline analysis.

Data were taken with different conditions of voltages, chamber orientations and magnetic field values. A scan was also made using different discriminating threshold values in the range from 2.4 to 5 fC. Below 2 fC, the rate of pulses generated by the noise of the amplifier itself starts to become important.

5.2. Test beam results without magnetic field

Fig. 8 shows a typical drift time spectrum and a distribution of the so called meantime (MT) obtained from the time of the signals (t_1, t_2, t_3) generated by the incoming muon in three consecutive, and staggered, layers using the expression $MT = (t_1 + t_3)/2 + t_2$. The smoothness of the drift time box and the fast drop of the trailing edge are a sign of the saturation of the drift velocity. The dispersion of the MT distribution (σ_{MT}) is a good stand alone measurement of the single cell time resolution (σ_t). Under the reasonable assumption that the time resolution is the same in all layers, $\sigma_t = \sqrt{\left(\frac{2}{3}\right)} \times \sigma_{MT}$. The position of the MT peak
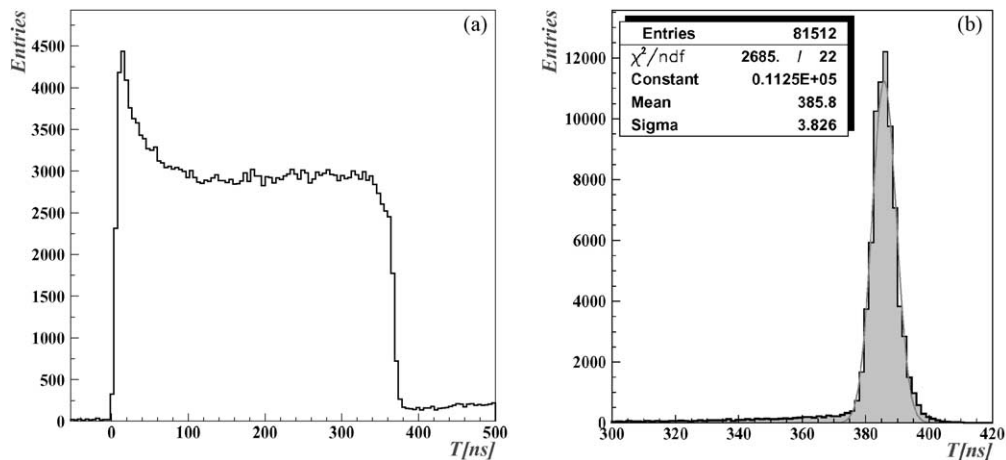

Fig. 8. A TDC spectrum as obtained from the raw data in a typical run during the test beam period can be seen in (a). A meantimer (MT) distribution can be seen in (b) together with the result of a Gaussian fit providing a sigma of 3.8 ns. From this value an average spatial resolution of 170 μm can be computed. The position of the MT peak allows to obtain an average drift velocity of 54.4 μm/ns. The tail on the left of the peak is due to delta rays.
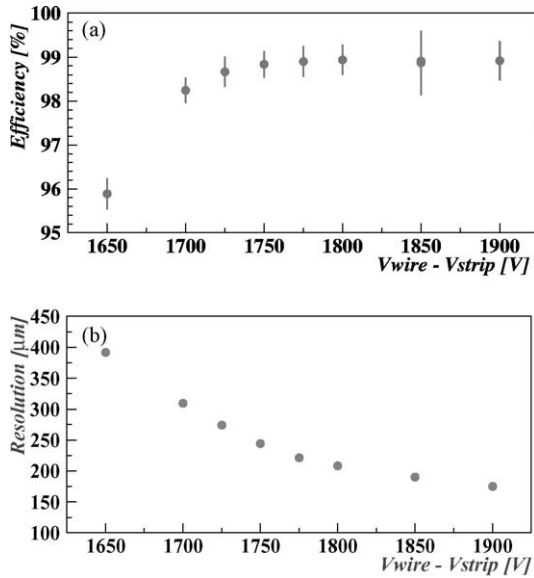
Fig. 9. Behaviour of the single wire efficiency (estimated as described in the text) (a) and resolution (b) as a function of $V_{ampl} = V_{wire} - V_{strip}$. The I-beams were set at -1.2 kV.
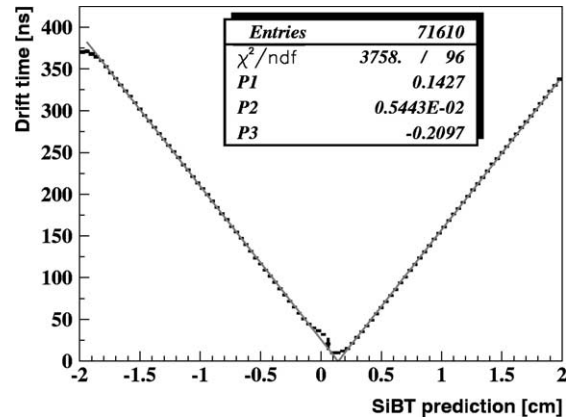

Fig. 10. Correlation between the chamber coordinate as extrapolated from the SiBT data and the time measured by Q4. From a straight line fit using the formula $t = \pm(x - P1)/P2 + P3$ a drift velocity of 54.4 μm/ns is obtained. The wire position is at 0.14 cm.

gives a measurement of the average maximum drift time, and consequently of the average drift velocity.

In Fig. 9, a typical efficiency curve can be seen together with a plot showing the variation of resolution, obtained from the MT distributions, as a function of the difference between wire and central strip voltages, V_{ampl}. The efficiency is computed here using the fraction of events, where hits in only three layers are seen. Since the beam was not perfectly perpendicular to the chamber plane, the effect of particles passing near the I-beams limits the efficiency to less than 100%. The knee of the plateau is reached around 1.75 kV. Already at this value the single wire resolution is better than the CMS requirement of 300 μm and it improves with the amplifying voltage. $V_{ampl} = 1.8$ kV was chosen as the reference value for the rest of the data taking and, after a scan on different I-beam voltages, reference voltage settings were fixed to -1.2, $+1.8$ and $+3.6$ kV for cathode, strips and wires, respectively.

Efficiency and resolution were found to be rather independent of the discriminating threshold, at least in the range from 2.4 to 5 fC. The

higher value, 5 fC, was considered to be a realistic threshold during LHC operation, and the rest of the data were collected under such condition.

Using the information of the Silicon Beam Telescope, the prediction of the muon track coordinates can be compared with Q4 measurements. The dispersion of the track impact position after extrapolation has been estimated to be around 300 μm, low enough to allow a reasonable measurement of the deviation from linearity due to a not completely uniform drift velocity. As shown in Fig. 10, the relation between distance to the wire and time is quite linear with the exception of one or two millimeters near the wire and also a small region close to the I-beam. The average value of the residuals, defined as the difference between the extrapolated coordinate and the value obtained from a constant drift velocity times the drift time measured by the chamber are plotted in Fig. 11, for two angles of incidence: 0° (perpendicular tracks) and 15°. Deviations from linearity are within ± 100 μm in most of the drift cell. These deviations are important for trigger purposes, that requires non-linearities below half the LHC bunch crossing separation of 25 ns: the observed deviations are smaller than 5 ns.

Single wire resolution is quite uniform as shown in Fig. 12, for different cells, as a function of the
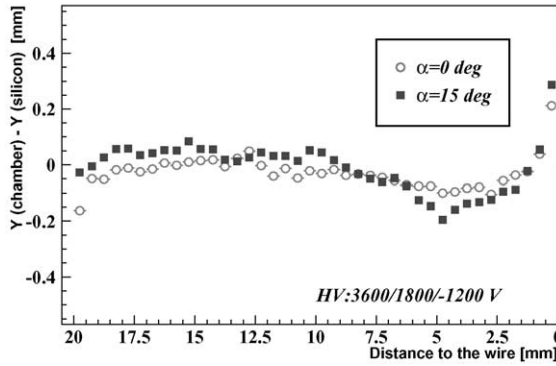
Fig. 11. Deviations from linearity as a function of the distance to the wire for tracks with $\alpha = 0°$ and $15°$. The I-beam is centered at 21 mm.
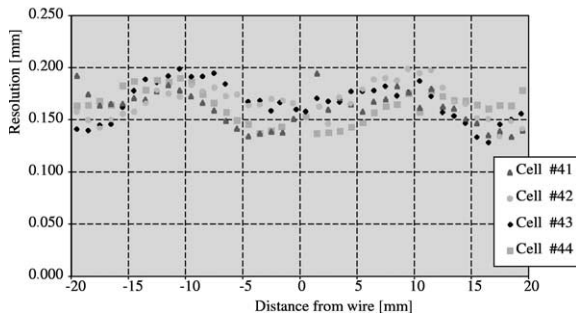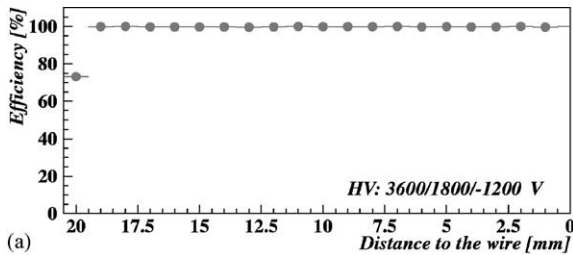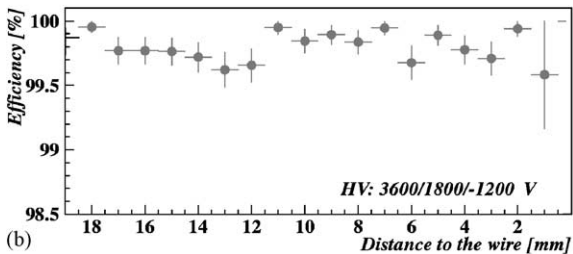

Fig. 12. Resolution as a function of the distance to the wire for a few different cells. The values obtained are in the range 0.15–0.2 mm and are rather uniform in all cells.

Fig. 13. Efficiency as a function of the distance to the wire (a); with an expanded scale excluding the I-beam region (b).
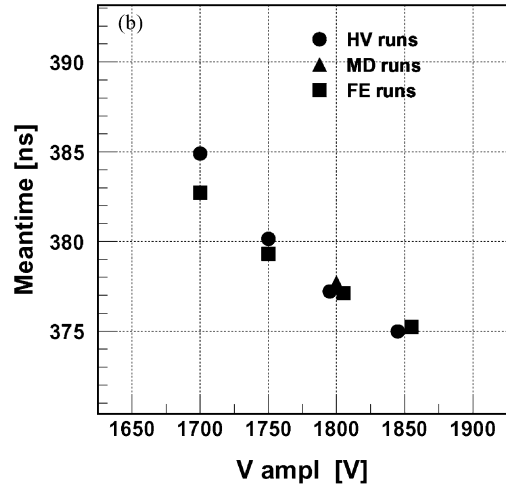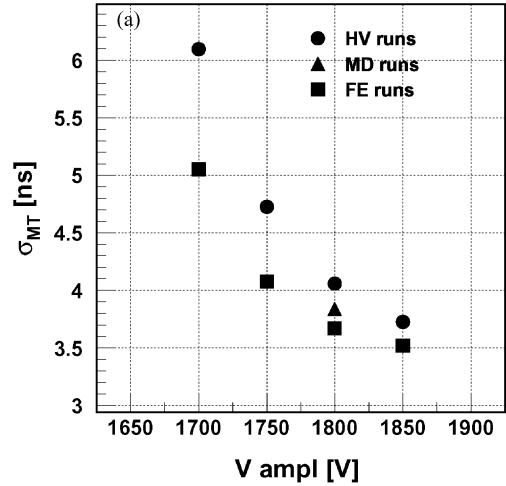

Fig. 14. Variation of the meantime resolution (a) and of the meantime value (b) with V_{ampl} at different beam hitting positions along the wire.

distance to the wire. All the values are between 150 and 200 μm.

Silicon Beam Telescope data can also be used to measure the chamber efficiency more precisely. The results are shown in Fig. 13. The geometrical acceptance associated to the presence of I-beams can be clearly seen by the drop of efficiency in that region. In the rest of the cell, the efficiency is always higher than 99.5%.

While during most of the runs, the beam was adjusted to intersect the central region of the

chamber wires (MD runs), some data were taken with the beam hitting in regions about 65 cm and 185 cm far from the end of the wire connected to the Readout electronics and symmetric with respect to the chamber centre (FE and HV runs, respectively). Effects of signal propagation along the wires could then be studied. As shown in Fig. 14a, the difference in resolution between HV and FE runs, due to signal dispersion, increases when a lower amplifying voltage is applied. The discrimination induces a dependence of the mean-time variable on the applied V_{ampl} as described in Ref. [1]. Fig. 14b shows that a steeper variation is obtained, as expected, for the HV runs. Operating the chamber at $V_{ampl} = 1800 \pm 50$ V the meantime variations are within ± 2.5 ns. From differences in the rise point of the drift time spectra, a value of $v = (2.56 \pm 0.17) \times 10^8$ m/s was estimated for the signal propagation velocity.

5.3. Test beam results with magnetic field

Because of the magnet yoke geometry in CMS, stray magnetic fields are present in the chamber regions. The expected behaviour of the radial and longitudinal components of the field, from computations of a two-dimensional model using a finite element analysis program (ANSYS), can be seen in Fig. 15. During the test Q4 was inside the superconducting magnet M1 in the H2 beam area. The magnetic field orientation was perpendicular to the beam direction and parallel to the chamber wires.

The distortion of the electron drift lines caused by a field of 0.5 T parallel to the wires can be seen in Fig. 16. This distortion can be roughly approximated by a rotation of the drift lines around the wire, simulating a rotation of the drift cell with respect to the direction of the incident particles. A change in the maximum drift path and time is generated, together with a drop of efficiency for inclined tracks which go through the I-beam region where the drift lines do not reach the wire. The staggering of the four layers minimizes the impact on track measurement of this last effect. In the case of a homogeneous magnetic field along the wire, the main consequence would be an effective lower drift velocity, but in CMS the magnetic field will not be homogeneous. Fig. 17 shows the drift velocity values obtained for several magnetic field values in the case of perpendicular tracks. A variation in the drift velocity of around 3% is observed from $B = 0$ to 0.5 T. This corresponds to a change in the maximum drift time of less than 12 ns, which is still acceptable.
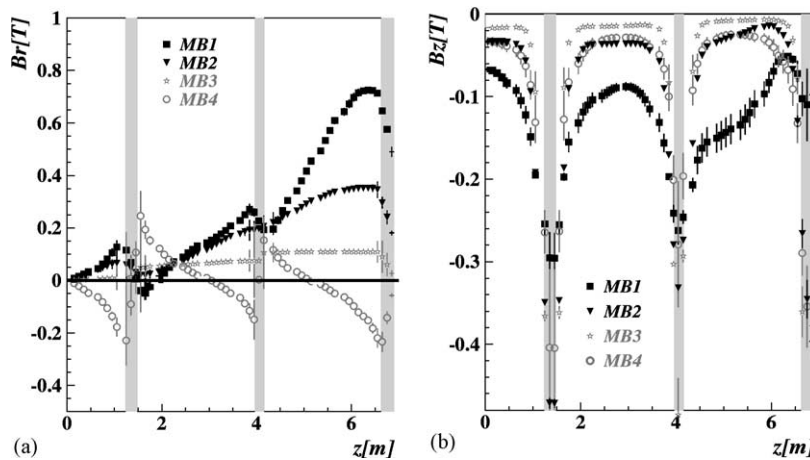

Fig. 15. Radial (B_r) and longitudinal (B_z) components of the CMS magnetic field in the regions where the barrel chambers will be placed as a function of the position along the beam direction (the center of the detector is at $Z = 0$). Vertical bands indicate the separation between chamber wheels (in these particular regions B_z becomes significant). The biggest B_r values (0.7–0.8 T) occur in the MB1 region near the endcaps.
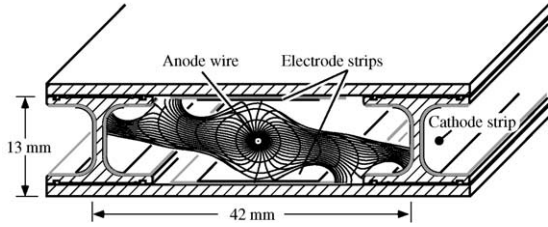
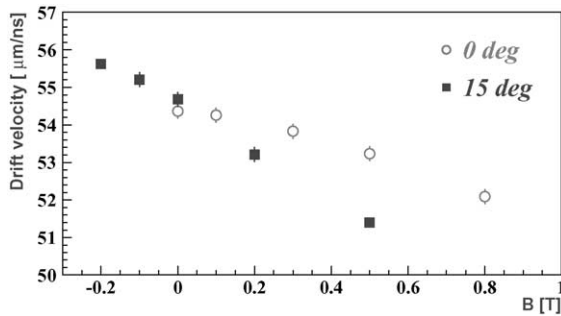Fig. 16. Simulation of the distortion produced in the drift lines by a 0.5 T magnetic field parallel to the wires.
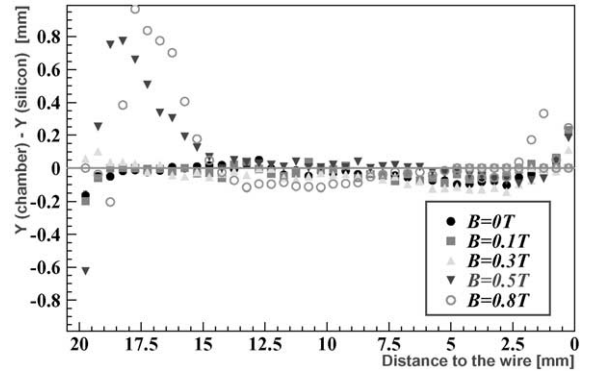

Fig. 18. Deviations from linearity as a function of the distance to the wire for several values of the magnetic field parallel to the wires in the case of perpendicular tracks. Big effects are seen for B fields of 0.5 T and higher.
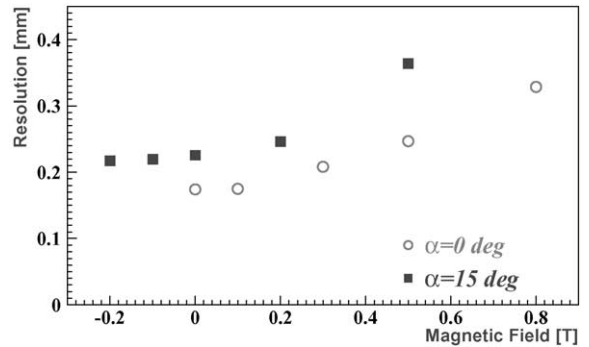

Fig. 17. Drift velocity for several magnetic fields for perpendicular (0°) and inclined (15°) tracks.

Fig. 19. Single cell resolution as a function of the magnetic field parallel to the wires for tracks with $\alpha = 0°$ and 15°. The constant average drift velocity of Fig. 17 is used for time to space conversion for each field value.

The effect on inclined tracks is more important as can also be seen in Fig. 17. Data were taken with the chamber inclined by 15° with respect to the beam and with the two magnet polarities (this is equivalent to keeping the same field and changing the incidence angle from 15 to −15°). At 15°, 0.2 T produces an effect similar to the one observed previously with perpendicular tracks at 0.5 T. The asymmetrical behaviour of the cell when reversing the magnetic field, already observed with previous prototypes [6], is really evident.

As shown in Fig. 18, the effects of the magnetic field on linearity are not very important below 0.3 T but increase dramatically for higher fields, mainly near the I-beams. The resolution is also slightly deteriorated by low magnetic fields. As shown in Fig. 19, the resolution is still better than 300 μm below 0.3 T. In CMS the magnetic field component parallel to the wires measuring the coordinate in the bending plane is expected to be below 0.1 T, with only very limited regions reaching 0.3 T. In such conditions, the results obtained confirm that the performance of the drift tube chambers will fulfill the expected requirements.

6. Conclusions

The first superlayer built with the first set of mass production tools has provided a confirmation of the estimated time and manpower needed for the construction of the CMS Barrel Muon

Drift chambers, as well as a verification of the quality of the tools. No major problems were met during the assembly, the setting up and the running of the chamber. Moved to the test beam with very little testing time, it operated immediately with a remarkable stability and without any problem at the lowest possible discriminating thresholds. The performance of Q4 is fully compatible with previous prototypes, and even significantly better in some respects. The beam test results validate the improved cell design and also the final versions of the Front End and Readout electronics.

References

[1] The CMS Muon Project, Technical Design Report, CERN/LHCC 97-32.

[2] F. Gonella, M. Pegoraro, Proceedings of the Fourth Conference on Electronics at LHC, CERN/LHC/98-36, pp. 257–261.

[3] P. Aguayo et al., Comparison between two possible CMS barrel muon readout architectures, CIEMAT Report 822, 1997.

[4] J. Christiansen, 32-channel general purpose time to digital converter. CERN/ECP–MIC, 1997.

[5] M. Benettoni, et al., Nucl. Instr. and Meth A 410 (1998) 133.

[6] M. Aguilar-Benitez, et al., Nucl. Instr. and Meth. A 416 (1998) 243.

[7] S. Bethke et al., CMS Note 1998/064.

[8] F. Gasparini et al., CMS IN-1999/005.

[9] M. De Giorgi et al., Proceedings of the First Workshop on Electronics for LHC experiments, CERN/LHCC/95-56, pp. 222–237.

[10] R. Veenhof, Garfield. A Drift Chamber Simulation Program User's Guide, CERN Program Library W5050, 1994.

[11] A. Benvenuti, et al., Nucl. Instr. and Meth. A 405 (1998) 20.

[12] C. Eklund, et al., Nucl. Instr. and Meth. A 430 (1999) 321.